FULL PAPER

Magnetic Resonance in Medicine 00:00–00 (2015)

# The Effect of Dissolved Oxygen on the Relaxation Rates of Blood Plasma: Implications for Hyperoxia Calibrated BOLD

Yuhan Ma,[1]* Avery J.L. Berman,[1,2] and G. Bruce Pike[2]

**Purpose:** To determine the contribution of paramagnetic dissolved oxygen in blood plasma to blood-oxygenation-level-dependent (BOLD) signal changes in hyperoxic calibrated BOLD studies.

**Methods:** Bovine blood plasma samples were prepared with partial pressures of oxygen ($pO_2$) ranging from 110 to 600 mmHg. $R_1$, $R_2$, and $R_2^*$ of the plasma with dissolved oxygen were measured using quantitative MRI sequences at 3 Tesla. Simulations were performed to predict the relative effects of dissolved oxygen and deoxyhemoglobin changes in hyperoxia calibrated BOLD.

**Results:** The relaxivities of dissolved oxygen in plasma were found to be $r_{1,\,O2} = 1.97 \pm 0.09 \times 10^{-4}$ $s^{-1}mmHg^{-1}$, $r_{2,\,O2} = 2.3 \pm 0.7 \times 10^{-4}$ $s^{-1}mmHg^{-1}$, and $r_{2,\,O2}^* = 2.3 \pm 0.7 \times 10^{-4}$ $s^{-1}mmHg^{-1}$. Simulations predict that neither the transverse nor longitudinal relaxation rates of dissolved oxygen contribute significantly to the BOLD signal during hyperoxia.

**Conclusion:** During hyperoxia, the increases in $R_2$ and $R_2^*$ of blood from dissolved oxygen in plasma are considerably less than the decreases in $R_2$ and $R_2^*$ from venous deoxyhemoglobin. $R_1$ effects due to dissolved oxygen are also predicted to be negligible. As a result, dissolved oxygen in arteries should not contribute significantly to the hyperoxic calibrated BOLD signal. **Magn Reson Med 000:000–000, 2015. © 2015 Wiley Periodicals, Inc.**

**Key words:** dissolved oxygen; relaxation rates; BOLD; hyperoxia

## INTRODUCTION

The calibrated blood-oxygenation-level-dependent (BOLD) method is a quantitative MRI technique to measure the cerebral metabolic rate of oxygen ($CMRO_2$), an important index of neuroenergetics and a biomarker of brain tissue viability (1,2). This method induces elevated BOLD signals by a mixed gas inhalation with additional $CO_2$ or $O_2$ to achieve conditions of hypercapnia or hyperoxia, respectively (3). Compared with hypercapnic calibration, hyperoxic calibration is more comfortable for subjects and has a minimal effect on cerebral blood flow (CBF), thus avoiding using a low signal-to-noise ratio perfusion imaging modality, such as arterial spin labeling (4,5). Carefully controlled hyperoxic-normocapnic calibration was also found to result in less variability in the estimated BOLD calibration constant (6). In addition, in recent years, the usage of hyperoxic calibration combined with hypercapnic calibration (dual-gas calibration) has become an emerging technique to assess baseline brain oxygen metabolism, therefore, providing valuable diagnostic and prognostic information on baseline brain tissue functions (7–10).

During a hyperoxic calibration, subjects breathe a gas mixture enriched with oxygen. After gas exchange at the lungs, the extra oxygen enters the arterial blood as dissolved gas because the hemoglobin is already nearly fully oxygenated. The extra oxygen dissolved in the arterial blood plasma is the first to be extracted into the brain tissue for aerobic metabolism, thereby reducing the dissociation rate of bound oxygen from the hemoglobin relative to normoxic conditions. As a result, the paramagnetic deoxyhemoglobin (dHb) concentration in the postarteriolar vascular compartments is decreased as compared to normoxic conditions. The process reduces the surrounding magnetic field inhomogeneity, thus shortening blood $R_2$ and $R_2^*$ to produce a positive BOLD response. This well-known phenomenon is the fundamental basis of BOLD functional MRI (11,12). However, in hyperoxic arterial blood, where the concentration of dHb is negligible, the effect of paramagnetic dissolved oxygen on the relaxation rates of blood plasma is less clear. If the dissolved oxygen in arterial blood plasma alters the relaxation rates significantly, it will confound the interpretation of hyperoxic calibrated BOLD, which assumes that the signal arises solely from the decreased concentration of dHb in capillary and venous blood.

Several studies have measured the variation in $R_1$, $R_2$, and $R_2^*$ of blood with hemoglobin oxygen saturation at different magnetic field strengths from 1.4 Tesla (T) to 11.7T (13–24). Under normal conditions, $R_2$ and $R_2^*$ decrease quadratically with increasing oxygen saturation levels in blood (13,19,21,25,26). However, during hyperoxia, dissolved paramagnetic oxygen can create microscopic field inhomogeneities that can increase the relaxation rates (27). Therefore, in arterial blood, where very little dHb is present during hyperoxia, the relaxation rates may increase due to dissolved oxygen, and these changes would oppose those occurring in partially deoxygenated venous and capillary blood. Hence, it is critical to characterize the contrast mechanism of

[1]McConnell Brain Imaging Centre, Montreal Neurological Institute, McGill University, Montreal, Quebec, Canada.

[2]Department of Radiology and Hotchkiss Brain Institute, University of Calgary, Calgary, Alberta, Canada.

*Correspondence to: Yuhan Ma, M.Sc., 3801 University Street, MNI, Room WB-325, Montreal, Quebec, Canada H3A 2B4. E-mail: yuhan.ma@mail.mcgill.ca

Received 28 August 2015; revised 5 October 2015; accepted 2 November 2015

DOI 10.1002/mrm.26069

Published online 00 Month 2015 in Wiley Online Library (wileyonlinelibrary.com).

dissolved oxygen in plasma to determine its impact in hyperoxic calibrated BOLD experiments.

The effects of dissolved oxygen on $R_1$, $R_2$, and $R_2^*$ of blood plasma in the absence of hemoglobin have not yet been investigated thoroughly and are generally ignored when arterial oxygen tension is < 350 mmHg (28). Gauthier and Hoge questioned whether hyperoxia induces an arterial signal by inspecting voxels that contain large arteries in $T_2^*$-weighted images and reported no signal changes in such (8). However, a recent theoretical study suggested that excess oxygen dissolved in arterial blood plasma can produce pronounced BOLD signal changes, thereby complicating the interpretation of the measured hyperoxia response and confounding its use in calibrated BOLD-based measurement of $CMRO_2$ (29). Our lab recently presented and experimentally validated a first principles derivation of the effects of dissolved oxygen on the susceptibility of plasma and predicted that it should not significantly alter the susceptibility values of blood within the ranges expected from hyperoxia (30). Another study at 4.7T reported significant changes in $R_1$ and $R_2$ of bovine serum with increasing oxygen tension (31). However, no direct measurements on the relaxation rates, in particular $R_2^*$, of blood plasma with dissolved oxygen have been reported at magnetic field strength of 3T, the most commonly used field strength for fMRI. Because of the paucity of experimental data on this subject, we aimed to resolve the question of whether the hyperoxic calibrated BOLD signal is contaminated by the paramagnetic effects of dissolved oxygen by means of direct experimental measurements.

This study investigates the effect of dissolved oxygen in bovine blood plasma by directly measuring longitudinal and transverse relaxation rates of the bovine plasma under various partial pressures of oxygen ($pO_2$). It complements our previous research on the effects of dissolved oxygen on the susceptibility of blood plasma (30). The relaxivities that we measure enable a straightforward prediction of the influence of dissolved oxygen on $T_2$*-weighted signals. The potential influence of dissolved oxygen on the hyperoxic calibrated BOLD signal is simulated using the measured relaxation rates and a detailed BOLD signal model (32).

## METHODS

### Sample Preparation

Bovine blood plasma (GeneTex, Inc., Irvine, CA) was used to mimic human blood plasma. The plasma contains 8 g/dL of protein, <2 mg/dL of Hb, and 8 g/L of trisodium citrate (Na-citrate) anticoagulant. All measurements were performed at room temperature of 296 to 297 K.

In this study, we used the same sample preparation procedure described in Berman et al (30). A 50-mL centrifuge tube was filled with bovine plasma to three quarters full. The centrifuge tube was then sealed with a rubber septum and self-adhesive Parafilm to maintain the desired $pO_2$. Two catheters were inserted into the rubber septum: one was connected to the pure medical $O_2$ supply to increase the $pO_2$ of the plasma; the other was used to outgas the air from the sample. $pO_2$ values ranging from 100 to 600 mmHg were achieved in the plasma samples by bubbling pure $O_2$ at a low flow rate (< 5 L/min) for 0–15 min. After reaching the desired $pO_2$, the oxygenated plasma was transferred into a 15-mL centrifuge tube sealed with a rubber septum and Parafilm.

The tube containing the oxygenated plasma solution was then positioned at the center of a 4-L watertight container filled with 20 μM $MnCl_2$ and 48 mM NaCl solutions. To reduce the susceptibility difference between the plasma sample and the surrounding background, 20 μM $MnCl_2$ was used, so that it is easier to achieve a homogeneous magnetic field through shimming (14). To match the conductivity of tissue and avoid radiofrequency (RF) penetration artifact, 48 mM NaCl was used (33,34).

After the plasma samples were transferred into the 15-mL centrifuge tube, the $pO_2$ of the remaining plasma sample in the 50-mL centrifuge tube was measured using an Orion Star A323 dissolved $O_2$ meter connected to a photoluminescence $pO_2$ probe (Thermo Fisher Scientific Inc., Waltham, MA). The photoluminescence $pO_2$ probe was inserted into the plasma sample while isolated from the surrounding air by sealing it using Parafilms.

### MRI Data Acquisition

All experiments were performed on a Siemens Tim Trio 3T scanner with a 32-channel RF receiver head coil. The phantom was positioned in the head coil such that the plasma tube was aligned approximately parallel to the $B_0$ field. A single 1-cm thick axial slice with an in-plane voxel size of 0.5 × 0.5 $mm^2$ was acquired near the isocenter. $R_1$ was measured using an inversion-recovery sequence with six inversion times (TI) = 30, 530, 1200, 2000, 3800, 5300 ms and repetition time (TR) = 6 s. $R_2$ was measured using a CPMG spin echo sequence with composite RF pulses and crusher gradients placed symmetrically around RF refocusing pulses to avoid stimulated echo effect (35). Thirty-two echoes were used for $R_2$ measurements with an echo spacing of 15 ms. $R_2^*$ was measured using a gradient echo sequence with 32 echoes at an echo spacing of 15 ms. Before each $R_2^*$ measurement, localized shimming (FASTESTMAP, Siemens) was performed on a 30 × 30 × 30 $mm^3$ volume centered on the acquired slice to minimize the macroscopic static field inhomogeneities that can enhance $R_2^*$ (36). For each $pO_2$, three measurements of $R_2$ and $R_2^*$ were repeated at three axial slice locations within 2 cm of the isocenter to account for variability in shimming and measurement errors.

### Image Analysis

A region of interest (ROI) containing only the plasma sample (approximately 20 voxels) was manually drawn on the acquired images. Relaxation rates of plasma were fitted on a voxel-by-voxel basis within the selected ROI using custom Matlab (The MathWorks, Inc., Natick, MA) scripts. For each repeated measurement, the average of $R_2$ and $R_2^*$ of all voxels within the ROI was calculated and used as the relaxation rates for that measurement. Under each $pO_2$, the reported final $R_2$ and $R_2^*$ of the plasma is the average of three repeated measurements. Because the $R_1$ measurement is less sensitive to the

macroscopic field inhomogeneity, only one measurement of $R_1$ was performed for each $pO_2$. $R_1$ was fitted from the inversion-recovery magnitude data using a general nonlinear least-squares model, which accounts for imperfect inversions and excitation flip angles (37). The reported $R_1$ is the voxel-wise average within the ROI at that $pO_2$.

To evaluate the effect of dissolved oxygen on the relaxation rates of the bovine plasma, relaxation rates were fitted using a total least-squares fitting script with respect to the measured $pO_2$. The slope of each fit was compared against the null hypothesis that there is no change in the relaxation rates as the $pO_2$ increases (i.e., the slope is zero) using the two-tailed t-test. Statistically significant results were reported when $P < 0.05$.

### Compensation for Diffusion Effect Due to the MR Imaging Gradients

Both the spin echo and gradient echo sequences used in our experiments consist of many magnetic field gradients. These gradients can lead to additional MR signal loss due to the diffusive motion of protons in water as described in the following equation (38):

$$S = S_0 e^{-t*R} e^{-bD} \quad [1]$$

where $S$ is the detected signal intensity, $S_0$ is the initial signal intensity, $R$ is the relaxation rate, $b$ is the sequence-specific diffusion-weighting factor, and $D$ is the diffusion coefficient of water protons. Here, we use $D = 2.299 \times 10^{-9}$ $m^2s^{-1}$ (39). $D$ in water is used because bovine plasma consists of 91% water (40).

In the spin-spin relaxation rate measurement, the signal loss due to the diffusion effect will increase the measured spin-spin relaxation rate as follows:

$$R_{app} = R_{int} + R_{diff} \quad [2]$$

where $R_{app}$ is the measured apparent relaxation rate, $R_{int}$ is the desired intrinsic relaxation rate, and $R_{diff}$ is the additional relaxation rate due to the diffusion effect.

In this study, the additional diffusion-related signal dephasing ($R_{diff}$) due to the imaging gradients in both the gradient echo and the spin echo sequences were taken into account. The diffusion b-factor was calculated for both the gradient echo and spin echo sequences by applying the Block-Torrey equation:

$$b = \gamma^2 \int_0^t dt'' \left[ \left( \int_0^{t''} \vec{G}(t')dt' \right) \cdot \left( \int_0^{t''} \vec{G}(t')dt' \right) \right] \quad [3]$$

where $\vec{G}(t)$ is the applied gradient in the sequence as a function of time and $\gamma$ is the gyromagnetic ratio. Because the blood plasma sample lacks restrictive microscopic structures, isotropic diffusion was assumed. The diffusion b-factor was calculated using Matlab scripts written in-house, taking the gradient waveforms as the input. The phase-encoding gradient was not used in the calculation because the zero phase-encoding should contribute the most to the final MR signal in the large, uniform, ROI we selected. After computing the b-factor, $R_{diff}$ was calculated as $R_{diff} = bD/t$ using a least-squares fitting algorithm, where $t$ refers to the echo times used in the experiment. The desired intrinsic relaxation rate $R_{int}$ was then calculated from Eq. [2].

### Simulations of the Calibrated BOLD Signal with the Effect of the Dissolved Oxygen

To evaluate the potential effects of changes in relaxation times induced by the dissolved oxygen in the arterial plasma on the measured hyperoxic calibrated BOLD signal, a detailed BOLD model was implemented to simulate the gradient echo signal (32). The detailed BOLD model (DBM) is a volume-weighted sum of BOLD signal from four compartments: the extravascular tissue signal and the three intravascular blood signals divided into arterial, capillary, and venous compartments. The overall BOLD signal change during a calibration or a stimulus is represented as:

$$\delta S = H[(1 - V_I)e^{-TE\cdot\Delta R^*_{2E}} + \varepsilon_A V_A e^{-TE\cdot\Delta R^*_{2A}} + \varepsilon_C V_C e^{-TE\cdot\Delta R^*_{2C}} + \varepsilon_V V_V e^{-TE\cdot\Delta R^*_{2V}}] - 1 \quad [4]$$

where

$$H = \frac{1}{1 - V_{I,0} + V_{A,0} + V_{C,0} + V_{V,0}}. \quad [5]$$

Here $V$ is the volume fraction of each compartment. The subscripts $E$, $I$, $A$, $C$, and $V$ represent extravascular, intravascular, arterial, capillary, and venous compartments, respectively. The subscript "0" defines the baseline values. The signal ratio of each intravascular compartment to the extravascular compartment is represented by the parameter $\varepsilon$. $\Delta R_2^*$ is the change of the $R_2^*$ relaxation rate for each compartment in the presence of a stimulus. Intravascular $\Delta R_2^*$ is calculated based on previous measurements of in vivo blood (19); whereas extravascular $\Delta R_2^*$ can be obtained following the procedures described in Griffeth and Buxton (32).

The DBM was then expanded to include the arterial plasma $R_1$ changes (DBM-$R_1$) with dissolved oxygen, as well as the arterial plasma $R_1$ and $R_2^*$ changes (DBM-$R_1$-$R_2^*$) due to dissolved oxygen during the hyperoxic calibrated BOLD experiment:

$$\delta S = H[(1 - V_I)e^{-TE\cdot\Delta R^*_{2E}} + \eta\varepsilon_A V_A e^{-TE\cdot\Delta R^*_{2A}} + \varepsilon_C V_C e^{-TE\cdot\Delta R^*_{2C}} + \varepsilon_V V_V e^{-TE\cdot\Delta R^*_{2V}}] - 1 \quad [6]$$

where

$$\eta = \frac{(1 - e^{-TR\cdot R_{1A,0}} e^{-TR\cdot\Delta R_{1A}}) \cdot (1 - e^{-TR\cdot R_{1A,0}}\cos\theta)}{(1 - e^{-TR\cdot R_{1A,0}} e^{-TR\cdot\Delta R_{1A}}\cos\theta)(1 - e^{-TR\cdot R_{1A,0}})}. \quad [7]$$

Here the parameter $\eta$ is the ratio of the signal at echo time (TE) = 0 with and without a stimulus. $\Delta R_{1A}$ is the change of the $R_1$ relaxation rate in the arterial blood with a stimulus. The parameter $\theta$ represents the flip angle. TR is the repetition time of the applied MRI sequence. To incorporate the effect of the change of the $R_2^*$ relaxation rate of the arterial blood plasma, $\Delta R^*_{2A}$ is also separated into two components: the change of $R_2^*$ caused by the

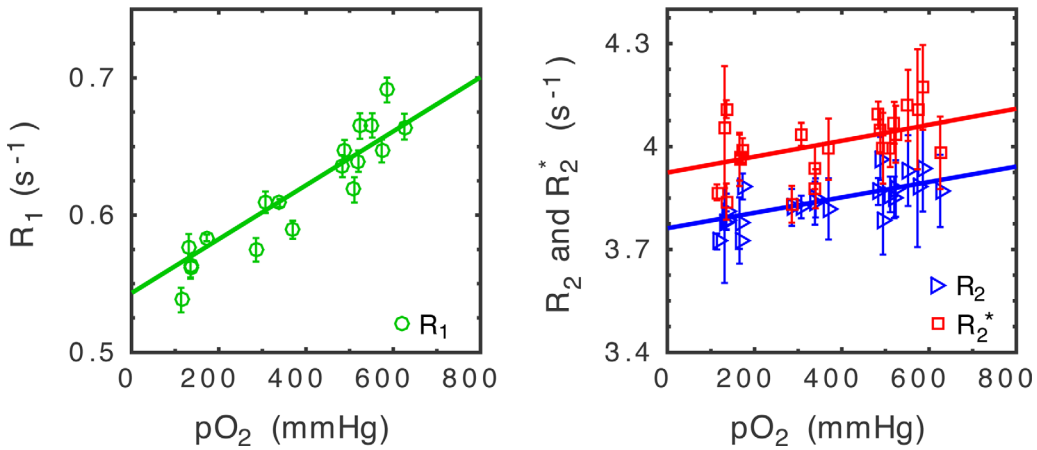


FIG. 1. Longitudinal (left) and transverse (right) relaxation rates of bovine plasma versus partial pressures of dissolved oxygen ($pO_2$).

oxygen saturation of hemoglobin ($\Delta R^*_{2A,Hb}$); and the change of $R_2^*$ in red blood cell (RBC) water and plasma water due to dissolved oxygen ($\Delta R^*_{2A,O2}$). Such that

$$\Delta R^*_{2A} = \Delta R^*_{2A,\ Hb} + (0.65\mathrm{Hct} + (1 - \mathrm{Hct}))r^*_{2A,O2} \cdot \Delta \mathrm{pO}_2 \quad [8]$$

where Hct is the hematocrit of arterial blood and (1 − Hct) represents the volume fraction of plasma. Because red blood cells consist of approximately 65% water, the volume fraction of water in red blood cells is calculated as 0.65Hct (41). $\Delta R^*_{2A,\ Hb}$ is computed for Hct of 0.44 as a function of arterial blood oxygen saturation level following the equation presented in Zhao et al (19). $r^*_{2A,O2}$ is the experimentally measured $R_2^*$ relaxivity of dissolved oxygen in plasma water, which is assumed equal for both RBC water and plasma water here. $\Delta pO_2$ is the difference in $pO_2$ under hyperoxia.

Three simulations were performed: first, the original DBM was simulated; second, the DBM was expanded with the parameter η to examine the effect of $R_1$; lastly, the DBM was expanded to include the parameter η and the two-compartment model of $\Delta R^*_{2A}$. For all three simulations, a standard hematocrit (Hct) of 0.44 and baseline oxygen extraction fraction ($OEF_0$) of 0.4 were assumed. Arterial $pO_2$ during the hyperoxic calibrated BOLD experiments was set between 210 and 610 mmHg, with a step size of 100 mmHg. We also assumed that no changes in CBF and $CMRO_2$ were induced during the hyperoxic calibrated BOLD experiments. Simulations were performed for 3T with the following sequence parameters: TE = 30 ms, TRs = 0.5 s and 3 s, the Ernst angle for gray matter was used as the flip angle with the gray matter $T_1$ taken as 1.3 s (42). The long TR of 3 s is the common TR used in the traditional fMRI acquisitions, whereas the short TR of 0.5 s was used to reflect emerging simultaneous multislice fMRI acquisitions (43). In addition to the relative BOLD signal change, the hyperoxic calibration parameter $M_{HO}$ was simulated as:

$$M_{HO} = \frac{\delta S}{1 - \left(\frac{[dHb]}{[dHb]_0}\right)^{\beta}} \quad [9]$$

where $[dHb]/[dHb]_0$ is the fractional reduction of the deoxyhemoglobin concentration in the venous vasculature due to the hyperoxic stimulus. The parameter β is a constant linking the blood oxygenation and the BOLD signal. Here β is chosen to be 1.3 for experiments at 3T (44). $[dHb]/[dHb]_0$ was calculated as described in Mark et al (6).

## RESULTS

$R_1$, $R_2$, and $R_2^*$ all linearly increased with increasing $pO_2$ and were fitted against $pO_2$ using a total least-squares fitting method (Fig. 1). From the slopes of the fits, the longitudinal and transverse relaxivities of the dissolved oxygen in plasma were found to be $r_{1,\ O2}$ =1.97 ± 0.09 ×$10^{-4}$ $s^{-1}mmHg^{-1}$, $r_{2,\ O2}$ =2.3 ± 0.7 ×$10^{-4}$ $s^{-1}mmHg^{-1}$, and $r_{2,\ O2}^*$ =2.3 ± 0.7 ×$10^{-4}$ $s^{-1}mmHg^{-1}$.

Testing the linear regressions against the null hypothesis $H_0$: slope = 0 yielded the *P*-values presented in Table 1. $R_1$, $R_2$, and $R_2^*$ were found to have statistically significant correlations with $pO_2$; however, the changes in $R_2$ and $R_2^*$ from baseline to a standard hyperoxic $pO_2$ of 410 mmHg were small (+2%), indicating that dissolved oxygen did not introduce substantial microscopic field inhomogeneities in blood plasma.

Measured $R_2^*$ and $R_2$ values were very similar, verifying that the residual macroscopic field inhomogeneities were negligible using the FASTESTMAP shimming technique. The fitted bovine blood plasma relaxation rates were corrected for the signal loss from the diffusion effect due to the magnetic gradients following the procedures described in the Methods section. For the spin echo sequence, the calculated additional diffusion-related signal dephasing ($R_{diff}$) was 0.15 $s^{-1}$. For the

Table 1
Coefficients of the Linear Regressions of R versus $pO_2$[a]

| | Slope ($10^{-4}$ $s^{-1}mmHg^{-1}$) | *P*-Value | $R^2$ |
|---|---|---|---|
| $R_1$ | 1.97 ± 0.09 | $3.7x10^{-13}$ | 0.85 |
| $R_2$ | 2.3 ± 0.7 | 0.0036 | 0.51 |
| $R_2^*$ | 2.3 ± 0.7 | 0.0027 | 0.24 |

[a]Testing the linear regressions against null hypothesis $H_0$: slope = 0 yields the *P*-values in the table. $R_1$, $R_2$, and $R_2^*$ are found to have statistically significant correlations with $pO_2$. $R^2$ is the coefficient of determination of the least squares linear fit.

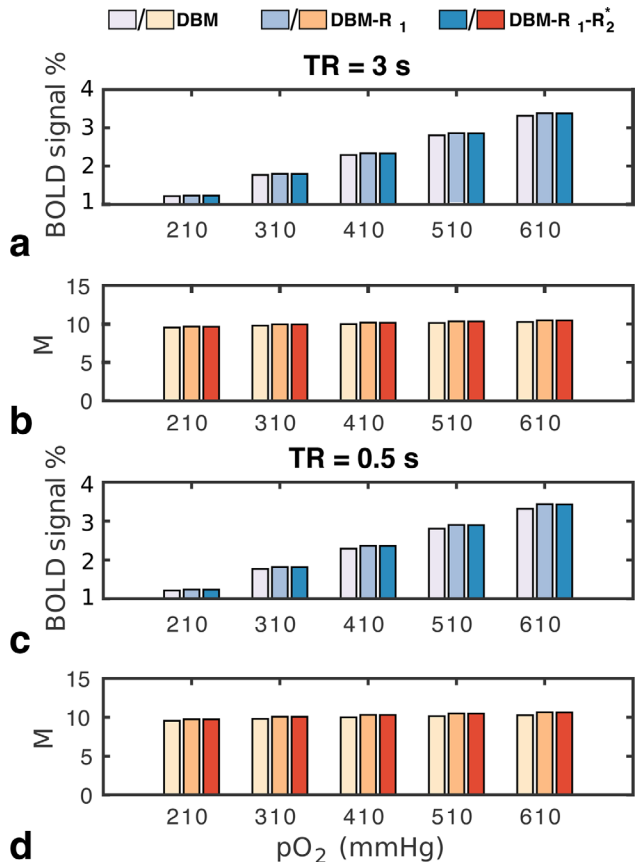


FIG. 2. Simulated hyperoxic calibrated BOLD signals from the detailed BOLD model (DBM), the detailed BOLD model incorporating the effect of the arterial plasma $R_1$ enhancement due to dissolved oxygen (DBM-$R_1$), and the detailed BOLD model incorporating the effect of both the arterial plasma $R_1$ enhancement and the arterial $R_2^*$ enhancement due to dissolved oxygen (DBM-$R_1$-$R_2^*$) with TR = 3 s (**a**) and TR = 0.5 s (**c**). Simulated BOLD calibration parameter M using the three DBMs with TR = 3 s (**b**) and TR = 0.5 s (**d**).

gradient echo sequence, the calculated additional diffusion-related signal dephasing ($R_{diff}$) was 0.03 $s^{-1}$. After correcting for $R_{diff}$, the intrinsic $R_{int}$ for $R_2$ and $R_2^*$ measurements were obtained (Fig. 1).

Simulations of the hyperoxia calibrated BOLD signal change using the DBM, DBM-$R_1$, and DBM-$R_1$-$R_2^*$ are shown in Figure 2. For the range of $pO_2$ (210 to 610 mmHg), the simulated relative BOLD signal increase was 1–3%; these increases were nearly identical for all three simulation schemes. For TR = 3 s, the average of the calibration parameter M across all ranges of $pO_2$ was found to be 10.0±0.3 for the DBM, 10.1±0.3 for DBM-$R_1$, and 10.1±0.3 for DBM-$R_1$-$R_2^*$. M calculated from DBM-$R_1$ and DBM-$R_1$-$R_2^*$ were not significantly different from M calculated from DBM (two-sample t-test yielded *P*: 0.61 and *P*: 0.61, respectively). When a TR of 0.5 s was used in the simulations, the $R_1$ effect became larger for higher $pO_2$ levels. For TR = 0.5 s, the average of the calibration parameter M across all ranges of $pO_2$ was 10.0±0.3 for the DBM, 10.3±0.4 for DBM-$R_1$, and 10.2±0.4 for DBM-$R_1$-$R_2^*$. Again, for this TR, M values calculated from DBM-$R_1$ and DBM-$R_1$-$R_2^*$ were not significantly different from M calculated from DBM (two-sample t-test yielded *P*: 0.22 and *P*: 0.40, respectively).

## DISCUSSION

This work presented the first experimental study of the effect of dissolved oxygen on $R_1$, $R_2$ and $R_2^*$ of blood plasma at the most commonly used field strength (3T) for calibrated BOLD fMRI. Our results suggest that the excess dissolved oxygen in arterial blood plasma during hyperoxic calibrated BOLD should not induce a significant arterial BOLD signal through $R_1$, $R_2$, and $R_2^*$ effects. We have shown that the changes in $R_2$ and $R_2^*$ from baseline $pO_2$ = 110 mmHg to standard hyperoxic $pO_2$ = 410 mmHg are very small (2%), indicating that dissolved oxygen did not introduce substantial microscopic field inhomogeneities in blood plasma. On the other hand, we observed that the dissolved oxygen enhances $R_1$ of the blood plasma, which can be attributed to the paramagnetic effect of oxygen molecules.

Putting our measured relaxation rates' changes into context with those generally observed in calibrated BOLD fMRI experiments, the maximal $R_2^*$ change in plasma due to dissolved oxygen was approximately one tenth of the $R_2^*$ change in venous blood typically observed during hyperoxic calibrated BOLD, assuming a hematocrit of 0.44 and baseline OEF of 0.4. In addition, under hyperoxic $pO_2$, the increases of the arterial plasma $R_2^*$ due to dissolved oxygen are around 0.6 to 1.7%, which are generally outweighed by the decreases of the arterial blood $R_2^*$ (around -3 to -4%) due to the binding of oxygen with the small remaining percentage of deoxygenated red blood cells (i.e., arterial $O_2$ saturation going from ~98% to 100%). The aforementioned comparisons are calculated based on the previous measurements of $R_2^*$ of whole human blood at 3T at various oxygen saturation levels (19). These comparisons further verify that under hyperoxia, the arterial BOLD signal changes do not have significant magnitude to influence the BOLD contrast that arises from changes in the concentration of dHb in the venous and capillary blood.

In contrast to our observation, a theoretical study suggested that significant BOLD signal change arises from the arteries, due to the paramagnetic effect of dissolved oxygen in blood plasma (29). However, that study overestimated the volume fraction of oxygen dissolved in plasma by using the volume fraction that oxygen occupies as a gas at the same $pO_2$, resulting in an overestimated BOLD signal. Measurements by Berman et al showed that the impact of dissolved $O_2$ on the susceptibility of the arterial blood plasma is negligible during the hyperoxic calibrated BOLD experiment (30). In the context of these two studies, our measured $R_2^*$ change is consistent with the susceptibility changes measured by Berman et al.

The enhancement of $R_1$ due to the paramagnetic effect of oxygen molecules is consistent with previous studies where the enhancement of $R_1$ was observed in arterial blood, fluid-rich tissues, and CSF under elevated oxygen tension (24,27,41,45–47). For instance, in the arterial blood with elevated oxygen tension, $R_1$ was found to increase linearly with increased oxygen tension (4). The

measured $R_1$ of the dissolved oxygen in the whole arterial blood agree with the dissolved oxygen in the blood plasma reported here. This is not surprising because the hemoglobin in the arterial blood is almost fully oxygenated, the blood plasma absorbs the majority of the dissolved oxygen, making the effect of dissolved oxygen in the arterial blood very similar to that in the blood plasma. Furthermore, because the commonly used perfusion imaging technique, arterial spin labeling (ASL), uses the blood $R_1$ in the quantification of CBF, the $R_1$ of blood plasma with dissolved oxygen quantified in this study can be used to improve the accuracy of CBF measurements under hyperoxic conditions. A brief ASL based calculation of CBF using the $R_1$ of arterial blood plasma quantified in this study (assuming arterial blood is fully oxygenated) revealed that if the enhancement of $R_1$ by dissolved oxygen is not taken into account properly, the resulting CBF will be underestimated by approximately 5% at the arterial $pO_2$ level of 410 mmHg. The calculation was based on the pseudocontinuous ASL technique with the parameters assumed from the "white" paper (48) and the CBF was assumed to remain the same at increasing $pO_2$ here. It is worth noting that previous studies that have reported CBF decreases during hyperoxia did so while incorporating a correction to $R_1$ in their CBF quantification (4,49). Therefore, their results likely represent a true decrease in CBF, not merely an underestimation of CBF if no $R_1$ correction was used.

In the hyperoxia calibrated BOLD method, the influence of this enhancement of $R_1$ in arterial blood plasma during hyperoxia has not been considered. Therefore, the BOLD signal was simulated using the detailed BOLD model proposed by Griffeth and Buxton (32). The DBM was expanded to take both $R_1$ and $R_2^*$ changes due to the dissolved oxygen in the arterial blood plasma into account. The simulation results showed minimal difference in both the relative BOLD signal and the calibration parameter calculated with the dissolved oxygen's effect, indicating that the dissolved oxygen induced relaxation rate changes are negligible. The effect of $R_1$ and $R_2^*$ changes will increase with shorter TRs and longer TEs. However, even for a short TR of 0.5 s, as commonly seen in the accelerated simultaneous multislice fMRI acquisition, there will be only a small increase in the relative BOLD signal due to the $R_1$ effect. Therefore, the influence of the dissolved oxygen in arterial blood plasma during hyperoxic conditions on the measured calibrated BOLD signal at 3T can generally be ignored.

In this work, we used FASTESTMAP shimming to minimize the macroscopic field inhomogeneities that can contaminate $R_2^*$ measurements. Without FASTESTMAP shimming, the gradient echo signal dropped quickly to the noise floor, making it impossible to correctly measure $R_2^*$ (data not shown). FASTESTMAP shimming before $R_2^*$ measurements led to a smooth exponential decay of $R_2^*$ values and enhanced the sensitivity of $R_2^*$ measurements to the possible microscopic field variations due to the dissolved oxygen molecules.

We have carefully taken the diffusion effect from water molecules into account for the $R_2$ and $R_2^*$ measurements. Although generally ignored, the imaging gradients in the multiecho sequence can induce extra diffusion weighting for water molecules. When the subject of study is an aqueous solution, the diffusion effect can lead to an apparent overestimation of the measured $R_2$ or $R_2^*$. To confirm the existence of the extra diffusion weighting due to the imaging gradients, we found that the measured $R_2$ increased with the increased refocusing intervals in the spin echo sequence (data not shown). This phenomenon is consistent with the $R_2$-dependency on the CPMG refocusing intervals in the presence of weak magnetic field inhomogeneities (50). Similarly, a recent study confirmed that the diffusion effect from the imaging gradients in the CPMG quantitative $T_2$ sequence does lead to the overestimation of $R_2$, which should be considered carefully in quantitative studies such as those measuring the myelin water fraction (51). In our study, the diffusion effect was accounted for by calculating the b-factor of both the gradient echo and spin echo sequences, assuming a diffusion coefficient of water, and correcting our $R_2$ and $R_2^*$ measurements accordingly.

## CONCLUSIONS

Our study found statistically significant increases in the relaxation rates $R_1$, $R_2$, and $R_2^*$ of the blood plasma with respect to increasing $pO_2$. However, the changes in $R_2$ and $R_2^*$ from baseline to standard hyperoxic $pO_2 = 410$ mmHg are quite small, approximately one-tenth of that in venous and capillary blood typically observed during a hyperoxic calibrated BOLD experiment. Furthermore, despite the effect of dissolved oxygen on the relaxation rates, our simulations of the calibrated BOLD signal and the calibration parameter under hyperoxia showed no significant difference when the dissolved oxygen relaxivities were accounted for or not. Our study verifies that, under hyperoxia, BOLD signal contrast is dominated by changes in the concentration of dHb in venous and capillary blood, the fundamental basis of the calibrated BOLD method, and not dissolved oxygen in arteries. This conclusion further solidifies the theoretical basis of the hyperoxic calibrated BOLD method and validates the application of the hyperoxic calibrated BOLD method in dual-gas calibration for the measurement of baseline brain oxygen metabolism.

## ACKNOWLEDGMENTS

The authors gratefully acknowledge the assistance of Raphael Paquin (Siemens) in setting up the FASTESTMAP shimming technique. Thanks are extended to Nikola Stikov, Mathieu Boudreau, and Jennifer Campbell for their insightful discussions.

## REFERENCE

1. Davis TL, Kwong KK, Weisskoff RM, Rosen BR. Calibrated functional MRI: mapping the dynamics of oxidative metabolism. Proc Natl Acad Sci U S A 1998;95:1834–1839.
2. Hoge RD, Pike GB. Oxidative metabolism and the detection of neuronal activation via imaging. J Chem Neuroanat 2001;22:43–52.
3. Pike GB. Quantitative functional MRI: concepts, issues and future challenges. Neuroimage 2012;62:1234–1240.
4. Bulte DP, Chiarelli PA, Wise RG, Jezzard P. Cerebral perfusion response to hyperoxia. J Cereb Blood Flow Metab 2007;27:69–75.

5. Chiarelli PA, Bulte DP, Wise R, Gallichan D, Jezzard P. A calibration method for quantitative bold fMRI based on hyperoxia. Neuroimage 2007;37:808–820.
6. Mark CI, Fisher JA, Pike GB. Improved fMRI calibration: precisely controlled hyperoxic versus hypercapnic stimuli. Neuroimage 2011; 54:1102–1111.
7. Bulte DP, Kelly M, Germuska M, Xie J, Chappell MA, Okell TW, Bright MG, Jezzard P. Quantitative measurement of cerebral physiology using respiratory-calibrated MRI. Neuroimage 2012;60:582–591.
8. Gauthier CJ, Hoge RD. Magnetic resonance imaging of resting OEF and CMRO(2) using a generalized calibration model for hypercapnia and hyperoxia. Neuroimage 2012;60:1212–1225.
9. Gauthier CJ, Desjardins-Crepeau L, Madjar C, Bherer L, Hoge RD. Absolute quantification of resting oxygen metabolism and metabolic reactivity during functional activation using QUO2 MRI. Neuroimage 2012;63:1353–1363.
10. Wise RG, Harris AD, Stone AJ, Murphy K. Measurement of OEF and absolute CMRO2: MRI-based methods using interleaved and combined hypercapnia and hyperoxia. Neuroimage 2013;83:135–147.
11. Ogawa S, Tank DW, Menon R, Ellermann JM, Kim SG, Merkle H, Ugurbil K. Intrinsic signal changes accompanying sensory stimulation: functional brain mapping with magnetic resonance imaging. Proc Natl Acad Sci U S A 1992;89:5951–5955.
12. Kwong KK, Belliveau JW, Chesler DA, et al. Dynamic magnetic resonance imaging of human brain activity during primary sensory stimulation. Proc Natl Acad Sci U S A 1992;89:5675–5679.
13. Thulborn KR, Waterton JC, Matthews PM, Radda GK. Oxygenation dependence of the transverse relaxation time of water protons in whole blood at high field. Biochim Biophys Acta 1982;714:265–270.
14. Barth M, Moser E. Proton NMR relaxation times of human blood samples at 1.5 T and implications for functional MRI. Cell Mol Biol (Noisy-le-grand) 1997;43:783–791.
15. Noseworthy MD, Kim JK, Stainsby JA, Stanisz GJ, Wright GA. Tracking oxygen effects on MR signal in blood and skeletal muscle during hyperoxia exposure. J Magn Reson Imaging 1999;9:814–820.
16. Spees WM, Yablonskiy DA, Oswood MC, Ackerman JJH. Water proton MR properties of human blood at 1.5 Tesla: magnetic susceptibility, t1, t2, t2* and non-lorentzian signal behavior. Magn Reson Med 2001;45:533–542.
17. Lu H, Clingman C, Golay X, van Zijl PC. Determining the longitudinal relaxation time (T1) of blood at 3.0 tesla. Magn Reson Med 2004; 52:679–682.
18. Stefanovic B, Pike GB. Human whole-blood relaxometry at 1.5 T: assessment of diffusion and exchange models. Magn Reson Med 2004;52:716–723.
19. Zhao JM, Clingman CS, Narvainen MJ, Kauppinen RA, van Zijl PC. Oxygenation and hematocrit dependence of transverse relaxation rates of blood at 3T. Magn Reson Med 2007;58:592–597.
20. Blockley NP, Jiang L, Gardener AG, Ludman CN, Francis ST, Gowland PA. Field strength dependence of R1 and R2* relaxivities of human whole blood to prohance, vasovist, and deoxyhemoglobin. Magn Reson Med 2008;60:1313–1320.
21. Chen JJ, Pike GB. Human whole blood T2 relaxometry at 3 Tesla. Magn Reson Med 2009;61:249–254.
22. Grgac K, van Zijl PC, Qin Q. Hematocrit and oxygenation dependence of blood (1)H(2)o T(1) at 7 Tesla. Magn Reson Med 2013;70:1153–1159.
23. Lin AL, Qin Q, Zhao X, Duong TQ. Blood longitudinal (T (1)) and transverse (T (2)) relaxation time constants at 11.7 Tesla. MAGMA 2012;25:245–249.
24. Rane SD, Gore JC. Measurement of T1 of human arterial and venous blood at 7T. Magn Reson Imaging 2013;31:477–479.
25. Spees WM, Yablonskiy DA, Oswood MC, Ackerman JJ. Water proton mr properties of human blood at 1.5 Tesla: magnetic susceptibility, T(1), T(2), T*(2), and non-lorentzian signal behavior. Magn Reson Med 2001;45:533–542.
26. Silvennoinen MJ, Clingman CS, Golay X, Kauppinen RA, van Zijl PC. Comparison of the dependence of blood R2 and R2* on oxygen saturation at 1.5 and 4.7 Tesla. Magn Reson Med 2003;49:47–60.
27. Tadamura E, Hatabu H, Li W, Prasad PV, Edelman RR. Effect of oxygen inhalation on relaxation times in various tissues. J Magn Reson Imaging 1997;7:220–225.
28. Berkowitz BA. Role of dissolved plasma oxygen in hyperoxia-induced contrast. Magn Reson Imaging 1997;15:123–126.
29. Schwarzbauer C, Deichmann R. Vascular component analysis of hyperoxic and hypercapnic bold contrast. Neuroimage 2012;59:2401–2412.
30. Berman AJ, Ma Y, Hoge RD, Pike GB. The effect of dissolved oxygen on the susceptibility of blood. Magn Reson Med 2015. doi: 10.1002/mrm.25571.
31. Song Y, Cho G, Chun SI, Baek JH, Cho H, Kim YR, Park SB, Kim JK. Oxygen-induced frequency shifts in hyperoxia: a significant component of bold signal. NMR Biomed 2014;27:835–842.
32. Griffeth VE, Buxton RB. A theoretical framework for estimating cerebral oxygen metabolism changes using the calibrated-bold method: modeling the effects of blood volume distribution, hematocrit, oxygen extraction fraction, and tissue signal properties on the bold signal. Neuroimage 2011;58:198–212.
33. Sled JG, Pike GB. Correction for B(1) and B(0) variations in quantitative t2 measurements using MRI. Magn Reson Imaging 2000;43:589–593.
34. Sled JG, Pike GB. Standing-wave and RF penetration artifacts caused by elliptic geometry: an electrodynamic analysis of MRI. IEEE Trans Med Imaging 1998;17:653–662.
35. Poon CS, Henkelman RM. Practical T2 quantitation for clinical applications. J Magn Reson Imaging 1992;2:541–553.
36. Gruetter R, Tkac I. Field mapping without reference scan using asymmetric echo-planar techniques. Magn Reson Med 2000;43:319–323.
37. Barral JK, Gudmundson E, Stikov N, Etezadi-Amoli M, Stoica P, Nishimura DG. A robust methodology for in vivo T1 mapping. Magn Reson Med 2010;64:1057–1067.
38. Stejskal EO, Tanner JE. Spin diffusion measurements: spin echoes in the presence of a time-dependent field gradient. J Chem Phys 1965; 42:288–292.
39. Holz M, Heil SR, Sacco A. Temperature-dependent self-diffusion coefficients of water and six selected molecular liquids for calibration in accurate 1H NMR PFG measurements. Phys Chem Chem Phys 2000;2:4740–4742.
40. Donnelly EB, Delaney RAM, Hurley N. Studies on slaughter animal blood plasma: I. Composition of bovine and porcine plasma. Irish J Food Sci Technol 1978;2:31–38.
41. Silvennoinen MJ, Kettunen MI, Kauppinen RA. Effects of hematocrit and oxygen saturation level on blood spin-lattice relaxation. Magn Reson Med 2003;49:568–571.
42. Wansapura JP, Holland SK, Dunn RS, Ball WS Jr. NMR relaxation times in the human brain at 3.0 Tesla. J Magn Reson Imaging 1999;9: 531–538.
43. Chen L, Vu AT, Xu J, Moeller S, Ugurbil K, Yacoub E, Feinberg DA. Evaluation of highly accelerated simultaneous multi-slice EPI for fMRI. Neuroimage 2015;104:452–459.
44. Ogawa S, Lee TM, Barrere B. The sensitivity of magnetic resonance image signals of a rat brain to changes in the cerebral venous blood oxygenation. Magn Reson Med 1993;29:205–210.
45. Young IR, Clarke GJ, Bailes DR, Pennock JM, Doyle FH, Bydder GM. Enhancement of relaxation rate with paramagnetic contrast agents in NMR imaging. J Comput Tomogr 1981;5:543–547.
46. Zaharchuk G, Busse RF, Rosenthal G, Manley GT, Glenn OA, Dillon WP. Noninvasive oxygen partial pressure measurement of human body fluids in vivo using magnetic resonance imaging. Acad Radiol 2006;13:1016–1024.
47. Remmele S, Sprinkart AM, Muller A, et al. Dynamic and simultaneous MR measurement of R1 and R2* changes during respiratory challenges for the assessment of blood and tissue oxygenation. Magn Reson Med 2013;70:136–146.
48. Alsop DC, Detre JA, Golay X, et al. Recommended implementation of arterial spin-labeled perfusion MRI for clinical applications: a consensus of the ISMRM perfusion study group and the European consortium for ASL in dementia. Magn Reson Med 2015;73:102–116.
49. Pilkinton DT, Hiraki T, Detre JA, Greenberg JH, Reddy R. Absolute cerebral blood flow quantification with pulsed arterial spin labeling during hyperoxia corrected with the simultaneous measurement of the longitudinal relaxation time of arterial blood. Magn Reson Med 2012;67:1556–1565.
50. Jensen JH, Chandra R. NMR relaxation in tissues with weak magnetic inhomogeneities. Magn Reson Med 2000;44:144–156.
51. Oakden W, Stanisz GJ. Effects of diffusion on high-resolution quantitative T2 MRI. NMR Biomed 2014;27:672–680.